Green Chemistry

PAPER

View Article Online
View Journal | View Issue

Cite this: *Green Chem.*, 2015, **17**, 869

Synergy of oxygen and a piranha solution for eco-friendly production of highly conductive graphene dispersions†

Keerthi Savaram,[a] Malathi Kalyanikar,[b] Mehulkumar Patel,[a] Roman Brukh,[a] Carol R. Flach,[a] Ruiming Huang,[a] M. Reza Khoshi,[a] Richard Mendelsohn,[a] Andrew Wang,[c] Eric Garfunkel[b] and Huixin He*[a]

A variety of strategies for the synthesis of solution processable graphene sheets has been developed so far. However, no approach has been reported to directly produce highly conductive, low-oxygen-containing graphene sheets without relying on toxic reagents and metal containing compounds and without generating toxic by-products. With an aim of developing such an eco-friendly approach, for the first time, this work studied solution phase oxidation of graphite particles and reversible graphite intercalation compounds using molecular oxygen and piranha etching solutions. We found that the synergy of the piranha etching solution and the intercalated molecular oxygen enables controlled oxidation of graphite particles assisted by microwave heating. The controlled oxidation leads to the rapid and direct generation of highly conductive, "clean", and low oxygen containing graphene sheets without releasing toxic gases or aromatic by-products as detected by gas chromatography-mass spectrometry (GC-MS). These highly conductive graphene sheets have unique molecular structures, different from both graphene oxide and pristine graphene sheets. It is even different from chemically reduced graphene oxide, while combining many of its merits. They can be dispersed in both aqueous and common organic solvents without surfactants/stabilizers, producing "clean" solution phase graphene sheets. "Paper-like" graphene films are generated *via* simple filtration, resulting in films with a conductivity of 2.3×10^4 S m^{-1}, the highest conductivity observed so far for graphene films assembled *via* vacuum filtration from solution processable graphene sheets. After 2 hours of low temperature annealing at 300 °C, the conductivity further increased to 7.4×10^4 S m^{-1}. This eco-friendly and rapid approach for the production of highly conductive and "clean" solution-phase graphene sheets would enable a broad spectrum of applications at low cost.

Received 9th September 2014,
Accepted 18th November 2014

DOI: 10.1039/c4gc01752h

www.rsc.org/greenchem

Introduction

Graphene has inspired a great deal of enthusiasm for over a decade. Due to its excellent electronic, thermal and mechanical properties along with its exceptionally large surface area and light weight, graphene holds great potential for a wide range of applications.[1,2] Fundamental studies and high-frequency electronics require pristine graphene.[3] "Bulk" applications such as batteries,[4–8] supercapacitors,[9] catalysts,[10,11] flexible macroelectronics,[12,13] and mechanically reinforced conductive coatings[14–16] require large quantities of highly conductive, solution-processable graphene manufactured at low cost. Mass production of conductive and solution processable graphene sheets, such as reduced graphene oxide (r-GO) and graphene nanoplatelets, has been recently achieved.[17–21] The majority of r-GO sheets have been fabricated *via* rather complex series of chemical processing steps. First, a lengthy process to oxidize graphite to graphite oxide is performed, which is followed by a thermal exfoliation process accompanied by partial deoxygenation (reduced). The exfoliated and partially reduced graphite is then dispersed into various solvents to obtain solution-processable r-GO.[22,23] Another commonly used approach to generate solution-proces-

[a]*Chemistry Department, Rutgers University, Newark, NJ 07102, USA. E-mail: huixinhe@rutgers.edu*
[b]*Department of Chemistry and Chemical Biology, Rutgers University, 610 Taylor Rd, Piscataway, NJ 0885, USA*
[c]*Ocean Nanotech LLC, 7964 Arjons Drive, Suite G, San Diego, CA 92126, USA*

† Electronic supplementary information (ESI) available: Data for larger scale production of Eco-ME-LOGr; concentration and production yield of the Eco-ME-LOGr in different solvents; lateral sizes and yields depending on microwave power; microwave irradiation time; O_2 purging time; and the H_2SO_4/H_2O_2 ratio; detailed mass spectra and possible assignment of the peaks showing on the GC spectrum of the filtrates at different retention times; principle and data treatment of thickness measurements *via* Rutherford backscattering spectroscopy (RBS). See DOI: 10.1039/c4gc01752h

sable r-GO is to first exfoliate and disperse the graphene oxide sheets in solution and then reduce the GO to a level that restores the conductivity of graphene. The widely used graphite oxidation methods, such as Staudenmaier,[24] Hofmann,[25] Hummers,[26] or Tour's methods,[27] all utilize metal containing oxidants, such as $KMnO_4$ and/or $KClO_3$. Trace residues of these oxidants and metal ions used or generated in these approaches can further participate in undesired reactions and can be detrimental to a wide range of applications.[14,28,29] However, purification of GO remains a challenge, mainly due to its tendency to gel. Even though these metal ions are water soluble, they were trapped due to the gelation tendency of GO, causing the GO product to be highly flammable.[29] Therefore, extensive cleaning and purification steps are required, making industrial scale production expensive and time-consuming.[27,30] Further during thermal exfoliation and deoxygenation of graphite oxide, it was believed that H_2O, CO and CO_2 gases were the only substances released during thermal exfoliation. However, a recent study demonstrated that a wide variety of complex organic molecules can also be released during processing, including alkanes, substituted polycyclic aromatic hydrocarbons, and heterocyclic molecules. The released molecules pose a potential hazard to our environment if not handled properly. Preventing the formation of these complex wastes is one of the greatest challenges for the graphene industry.[31] On the other hand, even though environmentally friendly reduction protocols are being developed to reduce dispersed graphene oxide,[30,32–35] hydrazine, a hazardous material, is still widely used as the reducing agent. Most importantly, these processes irreparably destroy the ideal honeycomb structure of graphene, leaving only a fraction of the properties of intrinsic graphene to be recovered.[36] Finally, except for those which are sulfonyl-functionalized[37] or reduced in basic solutions,[17,38,39] highly reduced GO sheets cannot be directly dispersed into water, which is the most useful and sustainable solvent. These sheets have been dispersed either in some organic solvents with high boiling points, such as *N*-methyl-pyrrolidone (NMP), or in aqueous solutions with the help of surfactants for stabilization.[38] Unfortunately, both the organic solvents and the surfactants are difficult to be completely removed from a graphene sheet surface without a high temperature annealing process. Residual solvent and surfactant species inevitably increase contact resistance between individual sheets in graphene films, reducing the overall electrical conductivity of graphene films produced using these chemistries.

Several research groups, including our own, have reported that defect-free graphene nanoplatelets can be directly produced from graphite particles and dispersed in NMP and other solvents, or aqueous solutions with the help of surfactants for stabilization.[19,21,40,41] Although the issue of releasing toxic gases was resolved, most of the production requires lengthy sonication and the yield is too low for practical industrial applications. Recently, a more scalable method to produce large-size pristine few-layered graphene was achieved *via* intercalation of metal containing compounds, followed by an interlayer exfoliation reaction.[18,42] These approaches are environmentally friendly and can be used for mass production of large and high quality graphene dispersion in NMP or pyridine, but unfortunately not in aqueous solutions due to the lack of oxygen containing groups on the basal plane of graphene. Therefore the issues associated with high boiling point solvents and trace quantities of metal ions remain.[29,43,44] Oh *et al.* explored an eco-friendly approach to directly produce graphene nanosheets from graphite particles without involving toxic and/or metallic compounds. However, the yield is too low (5%) for practical large scale production.[45]

We recently developed a fast, scalable oxidation approach without involving metallic compounds to directly and controllably produce highly-conductive graphene sheets that can be dispersed in both aqueous and organic solvents without the aid of surfactants.[46,47] In that work, $KMnO_4$ (as is used in Hummers and Tour's methods) was intentionally excluded, while nitronium aromatic oxidation combined with microwave heating (fast and local heating) was exploited. The unique process leads to a controllable oxidation of randomly positioned carbon atoms across entire graphene sheets, so that low density of oxygen containing groups were shown to be sufficient for exfoliation and dispersion into aqueous solutions. The dispersed graphene sheets, which we named as microwave-enabled low oxygen graphene (ME-LOGr), are highly conductive and do not require further reduction. Unfortunately, the use of nitronium ions results in the release of NO_2, a potentially toxic gas.

The current work aims to develop a more eco-friendly approach which retains the merits of the nitronium oxidation approach without releasing toxic gases or generating potentially toxic polycyclic aromatic hydrocarbons. This new approach replaces the mixture of H_2SO_4 and HNO_3 and exploits carbon oxidation chemistry by utilizing piranha solution, a mixture of H_2SO_4 and H_2O_2. Piranha solutions have been widely used in the semiconductor industry and research laboratories to clean silicon, glass, and gold and for oxidative cutting of carbon nanotubes (CNTs).[48,49] The reaction appears to generate only H_2O, O_2, and CO_2, without releasing toxic gases. However, the direct use of a piranha solution to oxidize graphite in fabricating large graphene sheets is less efficient than the use of the H_2SO_4–HNO_3 solution. This may be due to the rapid over-oxidation of the surface layers, in part related to the limited ability of the piranha constituents to access the inner graphene layers. This chemistry results in an uncontrolled cutting of graphene sheets at the surface and carbon loss *via* gasification. To solve these problems and to achieve controllable oxidization of each graphene layer, we first prepare a reversible H_2SO_4–graphite intercalation compound (GIC) with the help of $(NH_4)_2S_2O_8$ *via* a simple room temperature process.[50] This is followed by a short period of oxygen purging and microwave irradiation in piranha solution (Scheme 1). The synergy of the intercalated oxygen and the piranha solution enables controlled oxidation of graphite particles *via* microwave heating and thus leads to the rapid (60 seconds) and direct generation of highly conductive low oxygen containing graphene sheets. The intrinsic molecular oxidation mechanism leads to an eco-

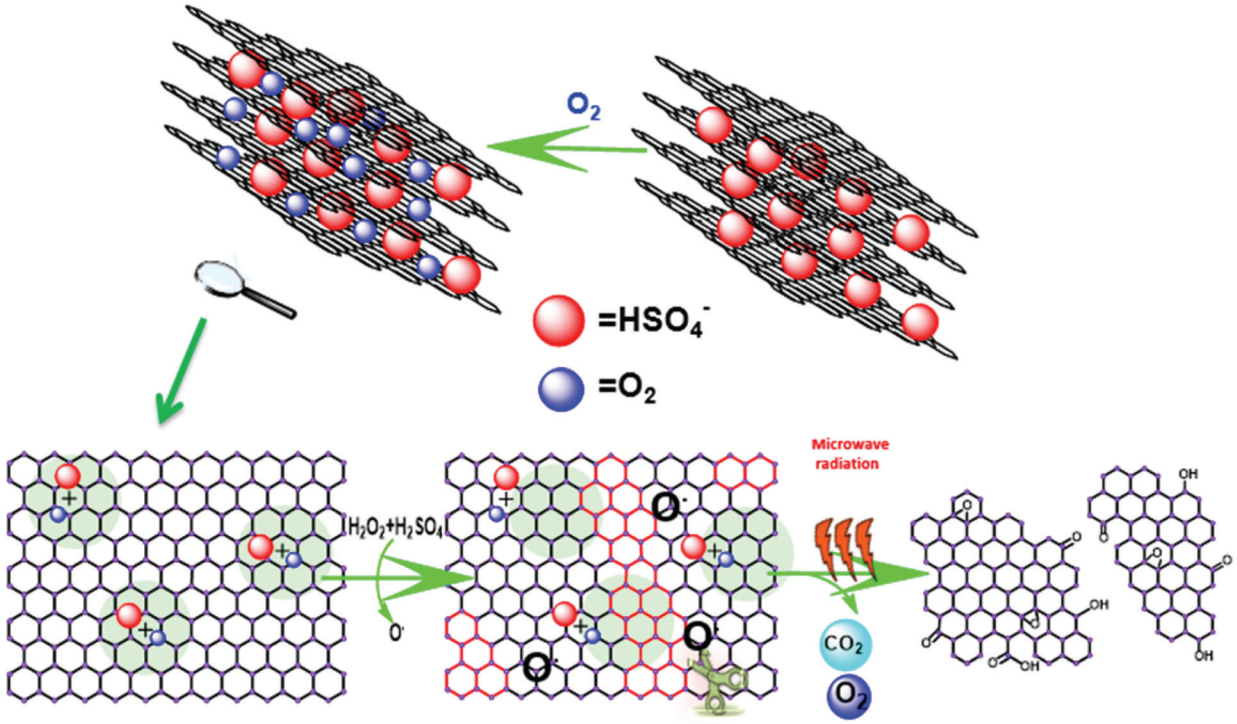

Scheme 1 Schematic drawing showing the process and oxidation mechanism of the proposed eco-friendly approach to directly produce highly conductive, low oxygen containing graphene sheets. A reversible H_2SO_4-GIC is formed by exposing graphite particles to a mixture of sulfuric acid and $(NH_4)_2S_2O_8$. The enlarged distance between the individual graphene sheets and the positive charges formed on their surfaces allow the purged molecular oxygen intercalating into the gallery of the graphene sheets in the GIC. Upon microwave irradiation in a piranha solution, the atomic oxygen generated from piranha and molecular oxygen intercalated inside the GIC synergistically oxidize the graphene sheets both inside and outside of the GIC particles without releasing toxic gases and generating aromatic small molecules as byproducts. This process rapidly generates enough epoxy and other oxygen containing groups, which facilitate exfoliation of highly conductive graphene sheets into water and other solvents without the requirement of post-reduction and surfactants for stabilization.

friendly fabrication of highly conductive graphene sheets without generating toxic byproducts, as demonstrated by GC-MS. To differentiate these films from the ME-LOGr that we generated previously by nitronium microwave oxidation, we refer to these graphene sheets as eco-friendly, microwave-enabled low-oxygen graphene (Eco-ME-LOGr). The Eco-ME-LOGr sheets are similar to the ME-LOGr in that they can be dispersed in various solvents, including in aqueous solutions, without needing surfactants for stabilization. The sheets are also highly conductive without requiring a post-reduction step. The conductivity of the as-fabricated Eco-ME-LOGr film is 2.3×10^4 S m^{-1}, the highest value reported so far for graphene films prepared from solution processable graphene sheets *via* simple vacuum filtration. After 2 hours of low temperature annealing (300 °C), the conductivity reaches 7.4×10^4 S m^{-1}. The electrical performance of the Eco-ME-LOGr films significantly outperformed the ME-LOGr films fabricated *via* nitronium microwave oxidation (6.6×10^3 S m^{-1} for as-prepared films and 1.9×10^4 S m^{-1} after 2 hours of annealing at 300 °C).[46]

Results and discussion

In a typical experiment, a reversible H_2SO_4-GIC (instead of H_2SO_4–HNO_3 GIC) is first formed by exposing graphite particles to a mixture of sulfuric acid and $(NH_4)_2S_2O_8$, following the recipes suggested by Tour's group.[50] The H_2SO_4-GIC was purged with O_2 for 5 minutes and then subjected to 60 seconds of microwave irradiation (CEM Discover, 300 watts, for smaller scale and Synthwave from Milestone, 900 W, for larger scale production, see details in the Experimental section and ESI, Fig. S1†) in a piranha solution. The reaction results in a finely dispersed suspension that is much easier to clean than the paste obtained using Hummer's method.[26] The dispersion was cleaned with water *via* vacuum filtration to remove residual H_2SO_4, $(NH_4)_2S_2O_8$, and any residual by-products.

With the help of bath sonication (30 min), the cleaned filtration cake can be re-dispersed in water to form a colloidal solution without using surfactants or stabilizers. The lateral size and thickness of the dispersed Eco-ME-LOGr sheets were characterized using a scanning transmission electron microscope (STEM), a scanning electron microscope (SEM), and an atomic force microscope (AFM). The thickness of the Eco-ME-LOGr sheets was found to be 0.7–3 nm, between one and a few layers. The sheets have an average lateral size of one to two micrometers with some as large as tens of micrometers across (Fig. 1), similarly to the ME-LOGr sheets reported earlier.[46]

The color of the Eco-ME-LOGr suspension is grayish-black. The UV-Vis-near infrared (NIR) spectrum of the Eco-ME-LOGr

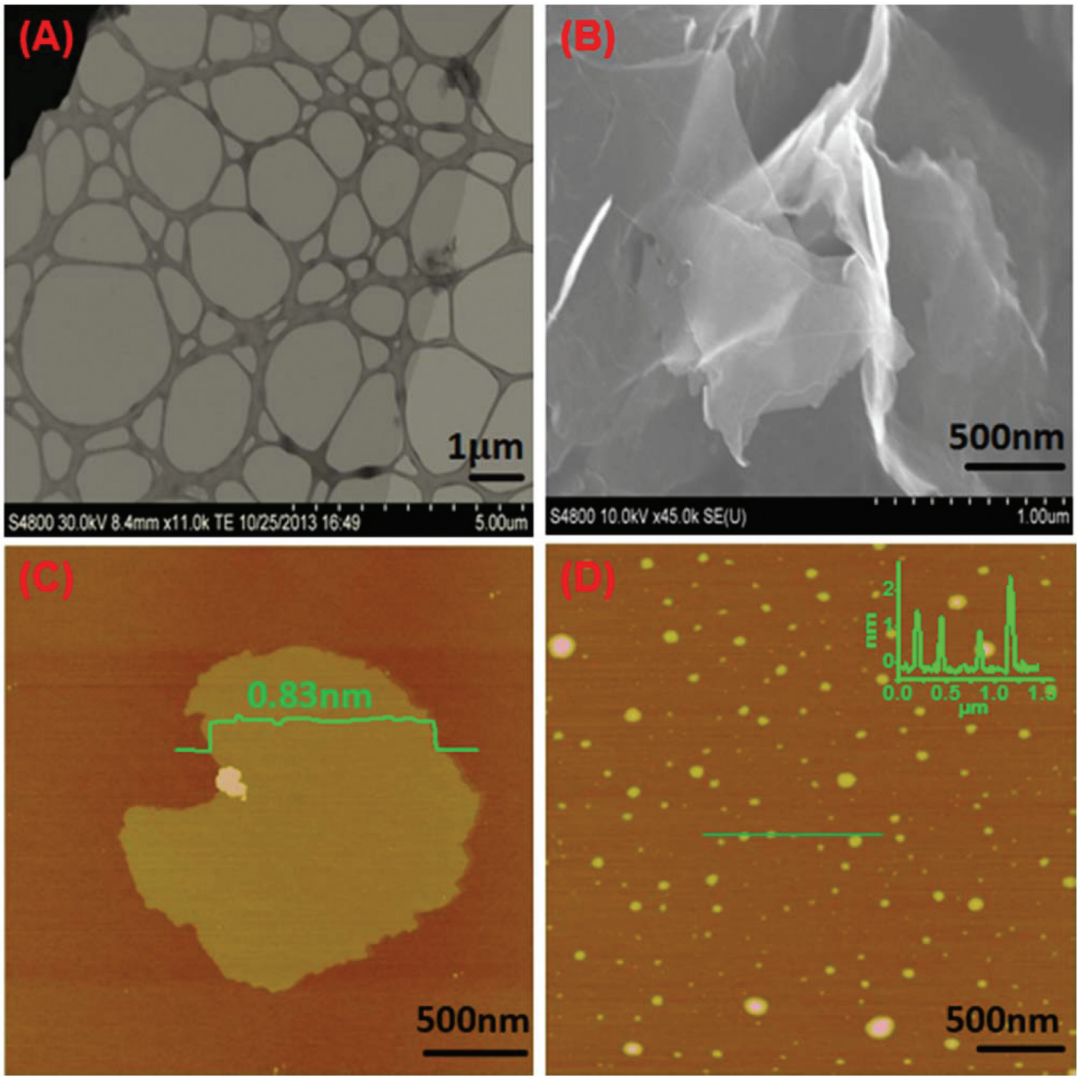

Fig. 1 Representative STEM, SEM and AFM images of the Eco-ME-LOGr fabricated *via* 5 min of O_2 purging of freshly prepared GIC, followed by 60 seconds of microwave irradiation in a piranha solution (A–C). Panel (D) shows an AFM picture of Eco-ME-LOGr sheets fabricated *via* microwave irradiation of graphite particles in a piranha solution.

solution displayed a plasmon band absorption maximum at a much longer wavelength than GO (268 nm *vs.* 230 nm) and much stronger absorption in the visible and NIR regions (Fig. 2A). All these characteristics are quite different from the typical brown GO solutions (Fig. 2A, inset),[17,51] yet similar to the previously reported r-GO and ME-LOGr suspensions. These features qualitatively suggest that the as-prepared Eco-ME-LOGr is also similar to the ME-LOGr sheets, containing a large amount of intact graphene domains without requiring a post-reduction procedure.[17,19,52]

Raman spectroscopy was utilized to estimate the size of the intact graphene domains. The typical G band, defect D band and 2D band features are shown in the Raman spectrum of the Eco-ME-LOGr film prepared on an anodisc filter membrane *via* vacuum filtration (Fig. 2B). The intensity ratio of D to G band (I_D/I_G) is 0.75, which is much lower than those of GO and r-GO,[30,51] indicating the high quality of the as-produced graphene sheets by this simple method. Furthermore, the Eco-ME-LOGr sheets also show a strong 2D band, suggesting that these sheets contain little adsorbent-induced surface contamination.[30,46]

In addition to water, the Eco-ME-LOGr sheets can also be dispersed in polar organic solvents such as NMP (290 mg L^{-1}) and *N*,*N*-dimethyl formamide (DMF) (200 mg L^{-1}), well known solvents to disperse intrinsic graphene sheets and graphene nanoplatelets. Interestingly, even in a nonpolar solvent such as chloroform, in which neither GO, r-GO, nor graphene platelets can be dispersed, the Eco-ME-LOGr can be dispersed with a concentration of 190 mg L^{-1}, ten times higher than that of the ME-LOGr sheets (Fig. 3 and Table S1 in ESI†).[46] It has been reported that the ability of graphene to be dispersed in various solvents is determined primarily by the surface functionalities of the graphene and Hansen parameters of the solvents. Good dispersibility can be reached when all three Hansen solubility

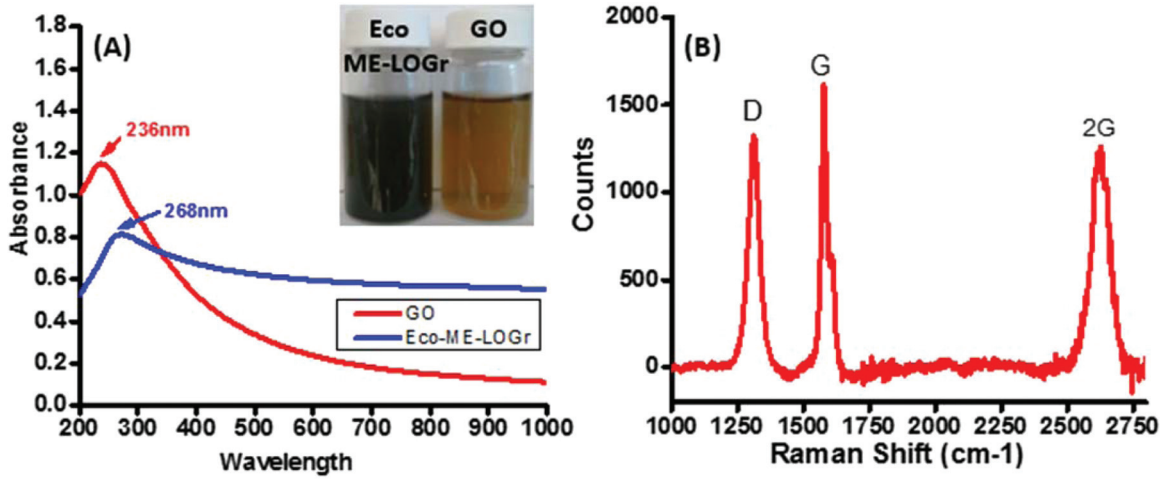

Fig. 2 (A) UV-Vis-near infrared spectroscopy of the Eco-ME-LOGr and graphene oxide dispersion in water and their digital pictures (inset). (B) Raman spectroscopy of the Eco-ME-LOGr films on the alumina anodic membrane.

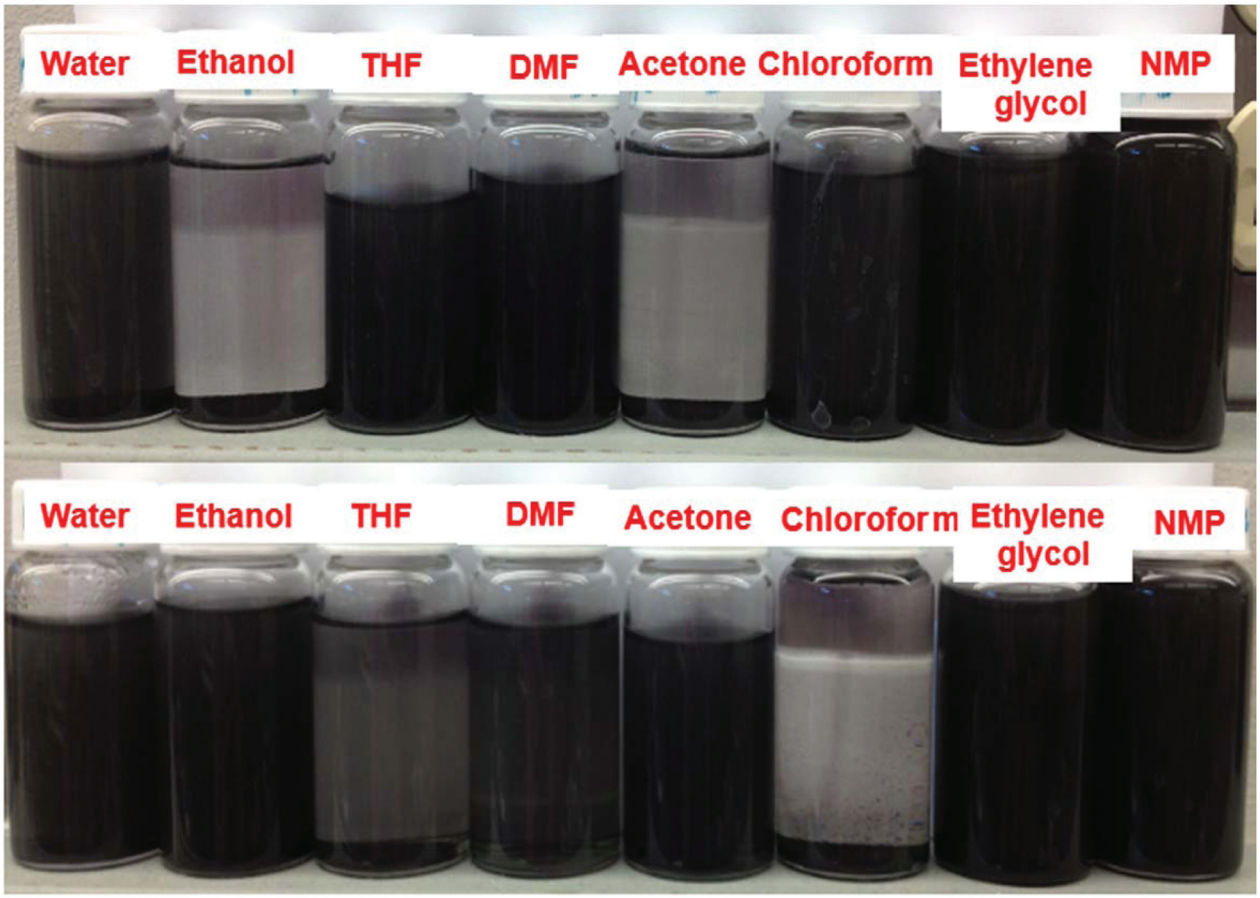

Fig. 3 Digital pictures of graphene dispersion in different solvents. The dispersions on the top were fabricated *via* the eco-friendly approach and the bottom ones were fabricated *via* nitronium oxidation.

parameters (dispersive, polar, and hydrogen-bonding) of a solvent match well with those of the graphene.[19,53] The high dispersibility in aqueous and organic (both polar and non-polar) solvents without requiring surfactants or stabilizers implies that the molecular structure (oxygen containing groups, their relative ratio and distribution on the surface) of the Eco-ME-LOGr sheets is quite different from previously reported GO, r-GO, and graphene nanoplatelets.[54,55] On the

other hand, ME-LOGr disperses well in ethanol and acetone, whereas the Eco-ME-LOGr is barely dispersed, indicating differences in their surface functionalities.[46]

The functional groups attached to the Eco-ME-LOGr sheets were studied by X-ray photoelectron spectroscopy (XPS). The C1s core-level XPS spectrum of Eco-ME-LOGr shows a main peak from oxygen-free carbon and a shoulder resulting from carbon bound to various oxygen species (Fig. 4A). The oxygen-free carbon makes up ~76% of the spectrum, similar to that observed for reduced GO sheets[54,55] and the ME-LOGr sheets reported previously.[46] However, the O1s spectrum of Eco-ME-LOGr is different from that of ME-LOGr (Fig. 4B and 4C). The O1s spectra for both the samples were deconvoluted to three or four peaks and their assignment is based on literature values.[56] The peak at 533 eV corresponds to oxygen present either as C–O in epoxides or anhydrides, or carboxylic groups (due to the very close overlap in binding energies of these functional groups, it is difficult to distinguish them from each other). The peaks at 532 and 531 eV were assigned to oxygen in hydroxyls and ethers along with carbonyl groups in esters and anhydrides, and oxygen in carbonyl groups attached to aromatic structures (quinone groups), respectively. From Table 1, it is apparent that the Eco-ME-LOGr contains more C–O components in epoxide, anhydrides, and carboxylic groups, whereas a higher percentage of carbonyl groups exists in the ME-LOGr.

The conductivity of the Eco-ME-LOGr sheets was also studied. It has been reported that the conductivity of graphene films formed from graphene dispersions exhibits percolation behavior.[57] The percolation threshold and the conductivity after percolation of graphene films are determined by the conductivity of the individual graphene sheets (itself a function of the extent of functionalization as well as their structure) and by their electrical connectivity (the number of contacts and the contact resistance between individual sheets in the films). Films of different thicknesses from the Eco-ME-LOGr aqueous suspension were prepared by vacuum filtration, a common technique to make relatively uniform films from solution phase graphene sheets.[55,58] Under a filtration-induced directional flow, graphene films are formed by stacking and interlocking of individual sheets.[55] After drying in a vacuum at room temperature, the average thickness of each film was estimated from the areal density of the films measured by Rutherford backscattering spectroscopy (RBS, see details in ESI†).[46] The sheet resistance of the films was measured with a four-probe approach. As shown in Fig. 5, the sheet resistance of the Eco-ME-LOGr film decreases with increasing film thickness. The electronic percolation of the Eco-ME-LOGr films was obtained at a thickness of ~88 nm, which has a sheet resistance of 0.5 kΩ per square, corresponding to a DC conductivity of 2.3×10^4 S m^{-1}. This conductivity is significantly higher than those of all of the chemically reduced GO films reported (see Table 2). It should be noted that the r-GO films listed here were obtained from stable r-GO aqueous suspensions without surfactants, so that their low conductivities are not due to surfactant or solvent effects.[17,38,39] The high quality of the Eco-ME-LOGr (the existence of larger intact graphene domains and fewer defects indicated by the low I_D/I_G ratio and the strong 2D band in its Raman spectrum) likely contributes to the observed high conductivity. This conductivity is also significantly higher than the graphene sheets directly exfoliated

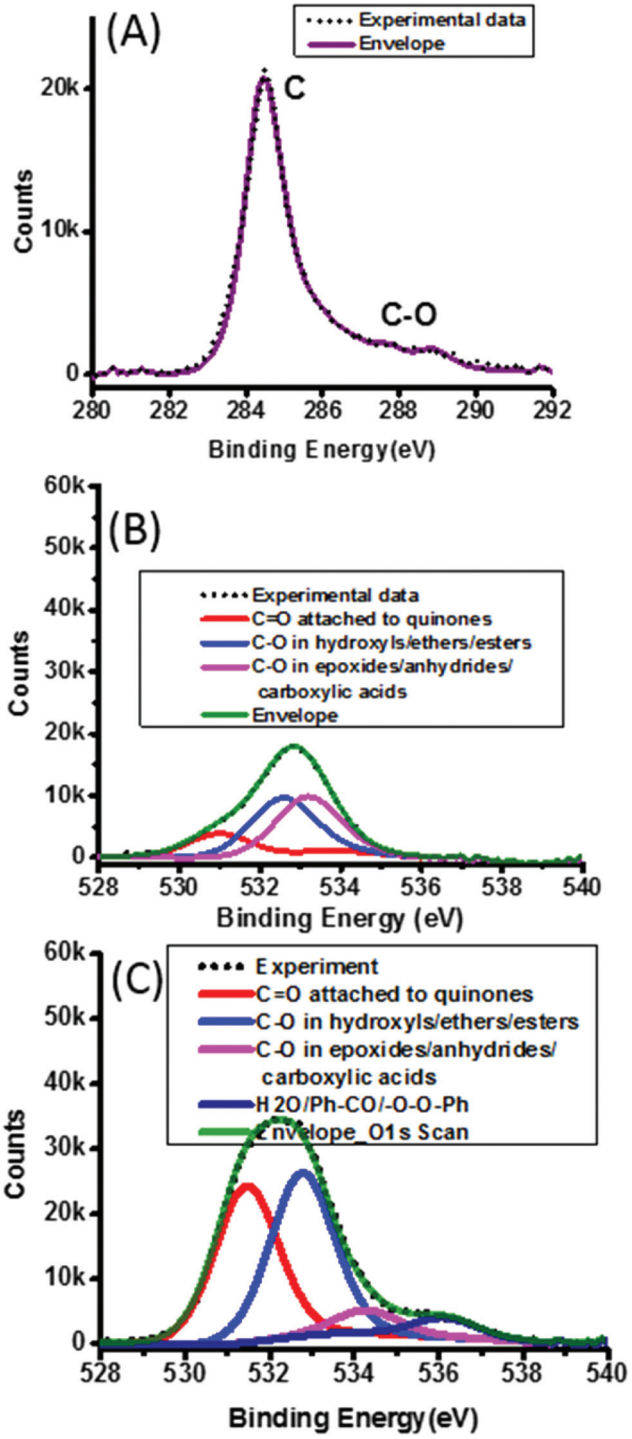

Fig. 4 XPS spectra of Eco-ME-LOGr films and ME-LOGr films on Au substrates. Panels (A) and (B) are C1s and O2p signals from the Eco-ME-LOGr films. The O2p signal from the ME-LOGr film is displayed here for comparison.

Table 1 Different oxygen containing groups in Eco-ME-LOGr and ME-LOGr

Functional groups	Binding energy (eV) of O1s	% of each component in Eco-ME-LOGr	% of each component in ME-LOGr
C–O in epoxide, anhydrides and carboxylic acids	533	41	6
C–O in hydroxyls and ethers, C–O with carbonyl groups in esters and anhydrides	532	42	45
C–O in carbonyl groups attached to aromatic structures (quinones)	531	18	43
Water	536	0	5

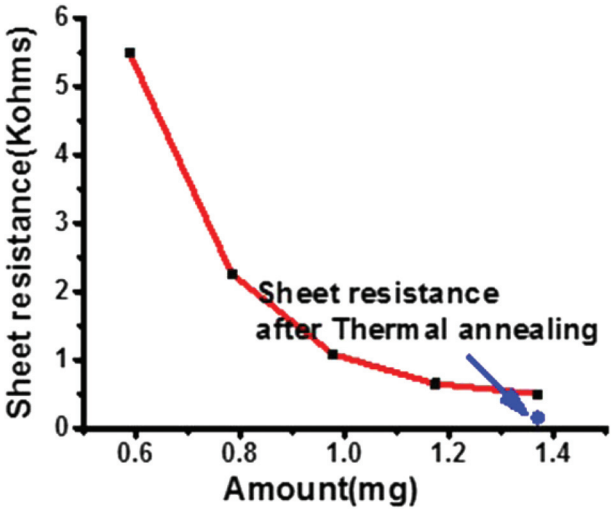

Fig. 5 Electronic percolation of the Eco-ME-LOGr films prepared by vacuum filtration.

in NMP and other organic solvents, as well as in aqueous solutions in the presence of surfactants/stabilizers, even though they were known to have lower defect densities.[19,41] The clean surface of Eco-ME-LOGr conveys better electronic communication between individual sheets when they were assembled into a film. Overall, the combination of the high conductivity of individual sheets and low inter-sheet contact resistance leads to the high conductivity of the Eco-ME-LOGr films.

Thermal annealing has been used to enhance the conductivity of graphene films by evaporating residual solvent/surfactant molecules, and/or thermal deoxygenation of the oxygen containing groups. Upon annealing the Eco-ME-LOGr film at 300 °C under Ar for 2 hours, the conductivity further increased to 7.44×10^4 S m^{-1}, which is significantly higher than those for similar r-GO films (Table 3). Although GO films can be directly converted to conductive films *via* thermal annealing, the electrical conductivity of thermally treated GO films was found to be much lower than annealed r-GO films.[58] Recently, the evolution of carbon bonds in GO films upon thermal annealing has been carefully studied by molecular dynamic simulations and *in situ* spectroscopic techniques (XPS and infrared spectroscopy) as a function of the initial oxygen density in GO films and annealing temperatures.[54,59] It was revealed that significant atomic rearrangement took place and the GO sheets were substantially disordered after thermal annealing, with the highest initial oxygen content resulting in the most severe distortion. In contrast, thermal annealing improved the ordering of the graphene sheets due to the initial low oxygen concentration of the chemically reduced GO films. It also gave rise to additional deoxygenation of the sheets. The improved ordering and the additional deoxygenation in the chemically reduced GO films have been ascribed to their higher conductivity than the directly annealed GO films.[38,58] It is noteworthy that the conductivity of the annealed Eco-ME-LOGr film at 300 °C is six times higher than that of the r-GO films annealed at 220 °C and two times higher than that of the r-GO annealed at 500 °C.[58] This result strongly

Table 2 Electrical conductivity of graphene films prepared *via* vacuum filtration of different solution phase graphene sheets

Fabrication techniques	Conductivity (S m^{-1})
Eco-ME-LOGr	22 600
ME-LOGr[42]	6600
Reduced graphene oxide *via* hydrazine under basic conditions[17,53]	7200
Reduced graphene oxide *via* hydrazine in the presence of pyrene derivatives[59]	200
Flash reduced GO[61]	1000
Reduced K-modified reduced GO[36]	690
Sulfonyl modified reduced graphene oxide in aqueous[34]	17
Electrochemical reduction of graphene oxide[60]	3500
Reduced GO in a variety of organic solvent mixtures[35]	1700
Solvothermal reduction of graphene oxide in NMP[14]	374
Graphene nanoplatelets in NMP[19]	5
Graphene nanoplatelets dispersed in aqueous solution *via* sonication with pyrene derivatives[37]	1900–2150
Graphene nanoplatelets dispersed in aqueous solution *via* sonication with sodium dodecyl benzene sulfate[38]	35

Table 3 Electrical conductivity of graphene films after low temperature thermal annealing

Graphene dispersion technique	Annealing temperature	Conductivity (S m^{-1})
Eco-ME-LOGr	300 °C for 2 h with Ar	74 400
ME-LOGr[42]	300 °C for 2 h with Ar	19 200
Reduced graphene oxide *via* hydrazine under basic conditions[17,53]	220 °C for 2 h with Ar	11 800
	500 °C for 2 h with Ar	35 100
Reduced GO in variety of organic solvent mixtures[35]	150 °C for 12 h	16 000
Solvothermal reduction of graphene oxide in NMP[14]	250 °C for 2 h	1380
Graphene nanoplatelets in NMP[19]	300 °C for 2 h with Ar	5000
	250 °C for 2 h with Ar/H_2	6500

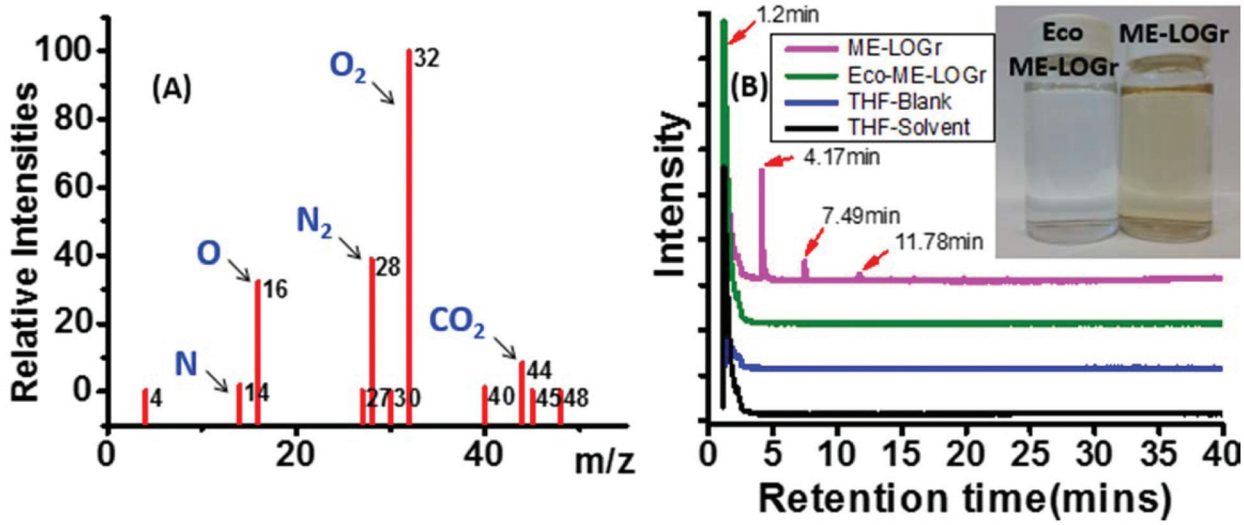

Fig. 6 (A) MS spectrum of the exhausted gas collected during microwave irradiation *via* the eco-friendly approach. (B) GC spectra of the filtrates collected during cleaning of the microwaved products. The curves from top to bottom are for the filtrates from nitronium oxidation, the eco-friendly approach, and a control experiment *via* the eco-friendly approach without adding graphite particles during microwave irradiation, and a pure THF solvent. Inset: Digital pictures of the two filtrates.

demonstrates that even though the oxygen content is similar to that in r-GO, the high quality (less defective structure) of Eco-ME-LOGr makes it much easier to recover the pristine electronic properties of graphene.

It should also be noted that the conductivity of the Eco-ME-LOGr films outperformed our ME-LOGr films as indicated by: a thinner percolation threshold (88 nm *vs.* 200 nm), lower sheet resistance at percolation threshold (0.5 *vs.* 0.76 kΩ per square), which corresponds to the much higher DC conductivity (2.26×10^4 S m^{-1} *vs.* 6.6×10^3 S m^{-1}) for as-prepared films. After 2 hours of annealing at 300 °C, the conductivity of the Eco-ME-LOGr films and the ME-LOGr films increased to 7.44×10^4 S m^{-1} *vs.* 1.92×10^4 S m^{-1}, respectively.[46]

We emphasize not only the significantly higher conductivity of the Eco-ME-LOGr films, but also that the chemistry to fabricate these high quality graphene sheets is eco-friendly without generating toxic gases and byproducts. First, we found that the gas released during the reaction was colorless, which was expected as no nitronium ions are involved in the piranha/O_2 oxidation approach. Surprisingly, the filtrate was also colorless, which is significantly different from the yellow/brown filtrates obtained from nitronium oxidation (Fig. 6B, inset). Gas chromatography-mass spectroscopy (GC-MS) was used to carefully study the composition of the released gas phase and the byproducts in the filtrates collected during cleaning of the microwave oxidized products. The gas phase collected during the microwave oxidation was directly injected into a GC-MS. The results show that the majority of the components were O_2 and a small amount of CO_2; no toxic SO_2 and CO were detected. Note that the 28 *m*/*z* peak is assigned to N_2 and not to CO as the GC-MS does not exhibit a strong carbon peak at 12 *m*/*z* which is characteristic of a CO spectrum (Fig. 6A).

To study the components in the filtrate (collected during cleaning of the microwaved product), it was first mixed with a low boiling point polar organic solvent such as tetrahydrofuran (THF) before injection. For comparison, the filtrate from nitronium oxidation and a blank solution (obtained by microwave irradiation of the same amount of $(NH_4)_2S_2O_8$ and piranha solution but without graphite particles) were also studied. In Fig. 6B, the chromatogram of the filtrate from nitronium oxidation shows several peaks at retention times of 1.5 min, 4.17 min, 7.49 min and 11.78 min. The mass spectra (MS) for each of the peaks were collected and are shown in ESI (Fig. S8†). The molecular structures associated with the peaks were identified based on the score (max. score is 1.00) of the MS compared to spectra in the mass bank database. The peak at 1.5 min is mainly from THF and the peak at 4.17 min is most likely from flavanol derivatives, while the peaks at 7.49 min and 11.78 min were due to relatively high molecular weight compounds like cyanine or 1,1′-dianthrimide. Detailed molecular structures and their scores are given in ESI (Table S3†). In marked contrast, the GC of the filtrate of the piranha oxidation approach is similar to that of the blank solution. Only one peak from the solvent (THF) itself was observed, demonstrating that this new piranha/O_2 oxidation approach is indeed eco-friendly without releasing any detectable toxic gases and generating any potentially toxic aromatic byproducts.

In general, an efficient approach to controllably fabricate graphene sheets from graphite requires the following conditions: (1) enabling the oxidant molecules to access internal surfaces of graphite particles (due to the strong interaction and close distance between the sheets, only the edges of graphite particles and the exposed graphene surface are

readily accessible to oxidants; the rest of the graphene is simply physically blocked from interacting with the oxidant molecules);[60] (2) ensuring that the reactions proceed in such a manner that oxygen containing groups (or other solubilizing groups) can be evenly (or at least randomly) placed across the graphene to have strong interactions with solvent molecules for dispersion; and (3) generating oxygenated groups in a controlled manner such that the process does not cut the graphene sheets into small pieces. In addition, the oxidation of each layer of graphene includes several steps: firstly, oxidation is initiated to create oxygen containing groups, such as –OH and/or epoxy groups, on the basal plane and edges of graphene sheets. Further oxidation includes two simultaneous and competing processes: (i) continuing initiation of oxidation in the intrinsic graphene domains resulting in the generation of more –OH and/or epoxy groups; and/or (ii) further oxidation of the already oxidized carbon atoms, ultimately leading to gasification of the carbon atoms (mostly CO or CO_2) and generation of small carbon residual species (which are separated during filtration), resulting in vacancies and holes throughout the graphene basal planes. This process is referred to as defect consumption or etching.[48,61] Consumption of the defects and generation of vacancies and holes in graphene sheets lead to rapid cutting of the CNTs into short pipes and cutting graphene sheets into small pieces.[48,49] The relative reaction rates of these processes determine the overall speed of the graphene fabrication and also the lateral sizes and oxidation level of the fabricated graphene sheets.

The molecular mechanism leading to all those different results compared to the nitronium oxidation approach needs further studies. We hypothesize that the difference arises due to their different intercalation capabilities, initial oxidation mechanisms and the following oxidization pathways. The mechanism for the nitronium oxidation approach is discussed in detail in our previous reports.[46] There is no detailed study of the piranha oxidation mechanism even though it has been used to oxidize and cut carbon nanotubes (CNTs).[49,62,63] It has been proposed that the most likely route by which piranha oxidation occurs is *via* the generation of atomic oxygen, which directly attacks a carbon in a graphene sheet to form a carbonyl group.[64] With the formation of carbonyl groups, the bonds of neighboring carbon atoms get disrupted. With further oxidation, the generated carbonyl group can be converted into CO_2, and simultaneously a new carbonyl group is created on a neighboring carbon atom. Compared to oxidation by nitronium ions, oxidation by piranha solution only generates water, CO_2 and O_2 as byproducts. If H_2SO_4–H_2O_2 can be used to oxidize graphite and fabricate graphene sheets, the issue of toxic by-products will be solved.

However, our results demonstrated that direct replacement of HNO_3–H_2SO_4 with piranha solution to efficiently fabricate conductive graphene in aqueous solution was not successful. The concentration of the dispersed graphene nanosheets is low (0.1 mg ml^{-1}). A majority of the graphite particles are precipitated out. This suggests that only small amounts of graphene sheets, which were located on the surface of the graphite particles, were oxidized. This result indicates that the atomic oxygen from the piranha solution is different from nitronium ions and has limited capability to reach and oxidize the internal sites of the graphite particles. Furthermore, most of the dispersed sheets are smaller than 200 nm, suggesting that the oxidized sheets were quickly cut into small pieces (Fig. 1D). It was reported that at room temperature H_2SO_4–H_2O_2 is not able to initiate oxidation of the graphene sidewall of carbon nanotubes, while it has a much faster speed to etch away the defects, thus cutting the tubes into small pipes compared to nitronium ions.[48,49] Even though the capability of H_2SO_4–H_2O_2 to initiate oxidation was increased with the microwave heating (a high reaction temperature was achieved), it is very possible that the etching speed increased more dramatically. As a result, the oxidized graphene sheets were quickly cut into small pieces.

To let the oxygen radicals access the inner parts of graphite particles, we thought of taking advantage of the enlarged distance between graphene sheets in a graphite intercalation compound (GIC). It was reported that exposing graphite powders to a mixture of $(NH_4)_2S_2O_8$ and H_2SO_4 at room temperature leads to formation of a reversible sulfuric acid-based GIC.[50] During GIC formation, positive charges were generated in the graphene sheets, which were balanced with intercalated HSO_4^- ions. Both HSO_4^- ions and H_2SO_4 molecules were intercalated in the interlayer galleries of the GIC. However, the efficiency of oxidation improved marginally, indicated by slightly increased graphene concentration (0.17 mg ml^{-1}), while the size of the sheets still remained very small (<200 nm) (ESI, Fig. S2A†). It was reported that the H_2SO_4-GIC formed from $(NH_4)_2S_2O_8$ is reversible since there were no C–O bonds formed. With water washing, the intercalated HSO_4^- and H_2SO_4 could be quickly de-intercalated.[50] Since the H_2O_2 solution contains 70% of water (by wt), possibly large amounts of HSO_4^{2-} and H_2SO_4 were already de-intercalated before the $O^{\bullet}$ radicals reach the inner graphitic particles.

To keep the enlarged distance in the GIC for $O^{\bullet}$ radical internalization, we purged O_2 to the freshly prepared GIC before exposing them to the piranha solution. We hypothesize that the distance between graphene sheets in the GIC is large enough for O_2 intercalation. Further, due to the high electronegativity of O_2, a strong attractive interaction between O_2 and the positive charges on the graphene sheets should exist, which would further facilitate O_2 intercalation and prevent its de-intercalation when the GIC is exposed to an aqueous environment. To study if purging O_2 would help to stabilize the GIC against de-intercalation, we compared the weight of the GICs with and without O_2 purging after water cleaning. The weight of the GIC with O_2 purging remained to a larger extent compared to that without O_2 purging, supporting our assumption (ESI, Table S2†). Therefore, it is very likely that the larger distances between graphene sheets in the GIC are largely retained compared to those without O_2 purging. Accordingly, oxidation of both internal and external graphene sheets in a graphitic particle is expected upon the addition of the piranha solution followed by microwave irradiation.

Furthermore, it was reported that trace amounts of C–O bonds were detected after keeping the reversible GIC in its parent $(NH_4)_2S_2O_8$–H_2SO_4 solution under ambient conditions for seven days.[50] Molecular level understanding of the chemical reaction of reversible GIC with oxygen in a highly acidic solution has not been extensively studied. We propose that the O_2 in air may intercalate and absorb around the positive charges, which can promote an electron/oxygen transfer reaction between the absorbed molecular oxygen and the positively charged graphene, leading to gradual generation of a few epoxy groups, a scenario similar to the nitronium ion intercalated GIC.[46] Considering that higher concentration of O_2 may be intercalated into the galleries of GIC along with the rapidly increased temperature *via* microwave heating, multiple oxygen containing groups can be efficiently generated not only along the edges, but also across the basal plane of graphene sheets *via* oxygen transfer reactions.[65,66] The synergy of intercalated oxygen and piranha may lead to increased speed in generating oxygen-containing groups relative to the cutting speed. Therefore, a higher yield of graphene production and less carbon loss were expected. Indeed, not only the concentration of graphene sheets is increased, but also the lateral sizes of the graphene sheet were also increased dramatically (Fig. 1).

A control experiment was performed by directly microwave heating the O_2 purged GIC without adding piranha solution. The results demonstrated that relatively larger graphene sheets were obtained compared to those obtained *via* piranha oxidation of GIC without O_2 purging. However, the obtained graphene sheets are much thicker while having smoother edges compared to those obtained in the presence of piranha solution (ESI, Fig. S3†). It should also be mentioned that purging O_2 directly to a mixture of H_2SO_4–graphite particles did not produce large graphene sheets, presumably due to the small distance between graphene sheets in graphite particles for O_2 intercalation. Furthermore, since there are no positive charges on graphene sheets in pristine graphite particles, there is no driving force for O_2 to internalize without forming a GIC in the first place. On the other hand, however, purging O_2 for longer times with a piranha solution and/or increasing the microwave irradiation time caused a significant decrease in the lateral sizes of the graphene sheets, or even more carbon loss, possibly due to over-oxidation induced cutting and etching (ESI, Fig. S4 and 5†).[48] In addition, the size and yield of the graphene sheets also depend on the ratio of H_2O_2–H_2SO_4 and the microwave power. Increasing the ratio of H_2O_2–H_2SO_4 and decreasing the microwave power result in deficient oxidation and most of the graphite particles precipitate out (ESI, Fig. S6 and 7†).

Finally, due to the different molecular oxidation mechanisms and their different kinetics in the initiation and the following oxidation pathways, we found that the role of microwave heating in these two approaches also varied. In the nitronium oxidation approach, microwave heating enables direct production of highly conductive graphene sheets without the requirement of a post-reduction process, while traditional heating results in nonconductive graphene oxide nanosheets. In contrast, both traditional heating and microwave heating lead to highly conductive graphene sheets *via* the piranha/O_2 oxidation chemistry. The graphene sheets produced *via* microwave heating are much larger (several μm) than those from traditional heating (<200 nm) (ESI, Fig. S2D†).

Conclusion

In summary, by the formation of reversible GIC, the distance between graphene sheets is increased simultaneously with the generation of positive charges on the graphene sheets, which provides enough space and imparts a strong attractive driving force for O_2 intercalation. The interaction between the positive charges and O_2 also helps in stabilizing the intercalated O_2 and HSO_4^- ions against de-intercalation upon the introduction of the piranha solution. The existence of the intercalated O_2 not only maintains the distance for piranha to access and oxidize the inner parts of graphite particles, but also acts as a mild oxidant to generate more oxygen containing groups on the graphene sheets which facilitates graphene sheet dispersion into aqueous solutions. The synergy of the piranha generated oxygen radicals, the intercalated O_2 and microwave heating enables rapid (60 seconds), direct and controllable fabrication of highly conductive graphene sheets of different lateral sizes without requiring a post-reduction procedure. The intrinsic oxidation mechanism of this new approach ensures that toxic by-products such as aromatic molecules or gases are not generated. Finally, the unique microwave heating not only enhances the fabrication process but also facilitates larger graphene sheet production compared to those utilizing traditional heating. Collectively, this approach has the following advantages for mass production of high quality graphene dispersions: (1) eco-friendly, no toxic agents are involved; (2) rapid and low energy consuming fabrication process; (3) direct production of graphene sheets of different lateral sizes without the requirement for a post-reduction process. The as-fabricated graphene sheets have a lower level of oxygen-containing groups, which ensures that the outstanding electrical and optical properties is maintained without the need for a high temperature annealing process;[54] (4) high-concentration dispersions both in aqueous and organic solvents (without requiring polymeric or surfactant stabilizers) allow a "clean" graphene surface to be obtained; (5) reduced waste from purification steps; (6) since only $(NH_4)_2S_2O_8$, O_2, H_2SO_4 and H_2O_2 are used for the production, the byproducts are essentially $(NH_4)_2SO_4$, and diluted H_2SO_4, which can be reused to produce more $(NH_4)_2SO_4$ as soil fertilizers. All these advantages ensure mass production of high quality graphene dispersions with low environmental footprints and at a much lower cost (the waste generated and energy consumed in the current process were roughly estimated and compared with other routine r-GO fabrications, clearly illustrating the green process reported in this work, see more details in the ESI†).

Experimental method

Materials

The Synthetic Graphite powder (size ≤20 μm) and ammonium persulfate (reagent grade, 98%) were obtained from Sigma Aldrich. The concentration of sulfuric acid used was 98% and was obtained from Pharmaco Aaper. The H_2O_2 is a laboratory grade solution with a concentration of 35 wt% obtained from BDH. All the chemicals were used as received. Extra dry grade O_2 was used for O_2 purging. The small-scale graphene synthesis was conducted *via* a CEM discover microwave vessel whereas the large scale synthesis was conducted *via* Synthwave from Milestone. Dispersion of the microwaved graphite powders to graphene sheets into various solvents was performed using a 5210 bath sonicator.

Eco-friendly approach for fabrication of graphene sheets

Graphite intercalation compound with SO_4^{2-} is produced by following the method described by Tour *et al.*[50] In brief, 1000 mg of ammonium persulfate [$(NH_4)_2S_2O_8$] was dissolved in 10 ml H_2SO_4. The obtained mixture solution was stirred for 5–10 min and then 200 mg of graphite powder was added. The obtained mixture was stirred for 24 h, which led to the formation of graphite intercalation compound (reversible SO_4^{2-}-GIC). To the GIC-SO_4 solution oxygen is purged for 5 min at a rate of 79–84 ml min^{-1}. 1 ml of the O_2 purged GIC-SO_4 solution is taken and mixed with 9 ml of piranha solution (H_2SO_4–H_2O_2 = 3 : 1), which is microwaved at 300 W for 60 s. The reaction is initially quenched with 200 ml deionized water. The obtained slurry was washed *via* vacuum filtration through a polycarbonate membrane with a pore size of 0.8 μm with 200 ml water each for four times. The final product is dispersed in 40 ml deionized water by sonication in a bath sonicator for 30 min. The solution is allowed to settle for 3–5 days and the supernatant solution obtained contains large graphene sheets. The filtrate is collected and then extracted with THF to study the byproducts *via* gas chromatography-mass spectrometry (GC-MS).

To demonstrate that this approach can be scaled up for mass production, 10 ml of the graphite intercalated solution, which is purged with O_2 for 5 min, is taken and to it 90 ml of piranha solution ($H_2SO_4 : H_2O_2$ – 3 : 1) is added and microwaved at 900 W for 60 s with Synthwave from Milestone. The quenching and cleaning of the product is similar to the small scale fabrication. The microwave enabled nitronium oxidation approach of graphene synthesis is conducted according to the procedure described in our previous work.[46] However the starting material is the graphite intercalated compound. The traditional heating of the piranha trial is conducted by heating 1 ml of O_2 purged GIC with 9 ml of piranha solution at 100 °C for 7 h and then quenching the reaction mixture with 200 ml deionized water and washing it with 200 ml water each for four times.

Characterization techniques

Surface morphology. The surface morphology of our as-fabricated product was characterized by atomic force microscopy using a Nanoscope IIIa multimode SPM (Digital Instruments) operated in "tapping mode" and by scanning electron microscopy (SEM) and scanning transmission electron microscopy (STEM) using a Hitachi S-4800 Field Emission Scanning Electron Microscope (FE-SEM, Hitachi Co. Ltd). The functional groups information was acquired using a Thermo Scientific Kα system with a monochromated Al Kα X-ray source ($h\nu$ = 1486.7 eV) in XPS. The quality of the graphene sheets was analyzed using Raman spectra with a Kaiser Optical Systems Raman Microprobe.

Optical and electronic properties. The optical properties of the graphene dispersions were measured by UV-VIS-NIR spectroscopy using a Cary-5000 Ultra violet-Visible-Near Infrared Spectroscope operated in double beam with the 200–1000 nm wavelength range. As for the electronic property assessment, the sheet resistance is measured using a manual four point resistivity probe from Lucas Laboratories, model 302. The conductivity of the films is calculated from the sheet resistance and thickness using the formula:

$$\text{Conductivity} = \frac{1}{\text{Sheet resistance} \times \text{thickness}}$$

Rutherford backscattering spectroscopy (RBS) was performed to calculate the thickness of the film to obtain the conductivity of the as-prepared graphene film, using a 2 MeV He^{2+} ion beam produced in a tandem accelerator with an ion current of 2–3 nA. Spectra were collected in the backscattering geometry and simulations were performed using the SIMNRA program (see details in ESI†).

Gas chromatography-mass spectrometry (GC-MS). The gas evolved during the reaction process and the filtrate during the cleaning procedure are carefully collected and analyzed using an Agilent HP6890 system, which was equipped with an HP-5-MS capillary column. The sample preparation procedure for the characterization techniques is discussed in detail in the ESI†.

Conflict of interest

The authors declare no competing financial interest.

Acknowledgements

This material is based on work supported by the National Science Foundation under grant no. STTR-1346496 (KS, AW and HH).

References

1 K. S. Novoselov, V. I. Fal'ko, L. Colombo, P. R. Gellert, M. G. Schwab and K. Kim, *Nature*, 2012, **490**, 192–200.

2 F. Bonaccorso, A. Lombardo, T. Hasan, Z. Sun, L. Colombo and A. Ferrari, *Mater. Today*, 2013, **15**, 564–589.
3 Y. Q. Wu, Y. M. Lin, A. A. Bol, K. A. Jenkins, F. N. Xia, D. B. Farmer, Y. Zhu and P. Avouris, *Nature*, 2011, **472**, 74–78.
4 K. Han, J. M. Shen, C. M. Hayner, H. Q. Ye, M. C. Kung and H. H. Kung, *J. Power Sources*, 2014, **251**, 331–337.
5 L. L. Jiang and Z. J. Fan, *Nanoscale*, 2014, **6**, 1922–1945.
6 H. Kim, H. D. Lim, J. Kim and K. Kang, *J. Mater. Chem. A*, 2014, **2**, 33–47.
7 A. H. Li, J. Q. Liu and S. Y. Feng, *Sci. Adv. Mater.*, 2014, **6**, 209–234.
8 N. Mahmood, C. Z. Zhang, H. Yin and Y. L. Hou, *J. Mater. Chem. A*, 2014, **2**, 15–32.
9 Z. J. Jiang, Z. Q. Jiang and W. H. Chen, *J. Power Sources*, 2014, **251**, 55–65.
10 Y. Zhu, S. Murali, M. D. Stoller, K. J. Ganesh, W. Cai, P. J. Ferreira, A. Pirkle, R. M. Wallace, K. A. Cychosz, M. Thommes, D. Su, E. A. Stach and R. S. Ruoff, *Science*, 2011, **332**, 1537–1541.
11 Z. Jin, W. Lu, K. J. O'Neill, P. A. Parilla, L. J. Simpson, C. Kittrell and J. M. Tour, *Chem. Mater.*, 2011, **23**, 923–925.
12 G. Eda and M. Chhowalla, *Adv. Mater.*, 2010, **22**, 2392–2415.
13 P. H. Wobkenberg, G. Eda, D. S. Leem, J. C. de Mello, D. D. C. Bradley, M. Chhowalla and T. D. Anthopoulos, *Adv. Mater.*, 2011, **23**, 1558–1562.
14 S. Dubin, S. Gilje, K. Wang, V. C. Tung, K. Cha, A. S. Hall, J. Farrar, R. Varshneya, Y. Yang and R. B. Kaner, *ACS Nano*, 2010, **4**, 3845–3852.
15 S. Stankovich, D. A. Dikin, G. H. B. Dommett, K. M. Kohlhaas, E. J. Zimney, E. A. Stach, R. D. Piner, S. T. Nguyen and R. S. Ruoff, *Nature*, 2006, **442**, 282–286.
16 T. Ramanathan, A. A. Abdala, S. Stankovich, D. A. Dikin, M. Herrera-Alonso, R. D. Piner, D. H. Adamson, H. C. Schniepp, X. Chen, R. S. Ruoff, S. T. Nguyen, I. A. Aksay, R. K. Prud'homme and L. C. Brinson, *Nat. Nanotechnol.*, 2008, **3**, 327–331.
17 D. Li, M. B. Muller, S. Gilje, R. B. Kaner and G. G. Wallace, *Nat. Nanotechnol.*, 2008, **3**, 101–105.
18 X. Geng, Y. G. Guo, D. Li, C. Zhu, X. Wei, M. N. Chen, S. Gao, S. Qiu, Y. Gong, L. Wu, M. Long, M. Sun, G. Pan and L. Liu, *Sci. Rep.*, 2013, **3**, 1134.
19 Y. Hernandez, V. Nicolosi, M. Lotya, F. M. Blighe, Z. Y. Sun, S. De, I. T. McGovern, B. Holland, M. Byrne, Y. K. Gun'Ko, J. J. Boland, P. Niraj, G. Duesberg, S. Krishnamurthy, S. Goodhue, J. Hutchison, V. Scardaci, A. C. Ferrari and J. N. Coleman, *Nat. Nanotechnol.*, 2008, **3**, 563–568.
20 S. Park and R. S. Ruoff, *Nat. Nanotechnol.*, 2009, **4**, 217–224.
21 K. R. Paton, E. Varrla, C. Backes, R. J. Smith, U. Khan, A. O'Neill, C. Boland, M. Lotya, O. M. Istrate, P. King, T. Higgins, S. Barwich, P. May, P. Puczkarski, I. Ahmed, M. Moebius, H. Pettersson, E. Long, J. Coelho, S. E. O'Brien, E. K. McGuire, B. M. Sanchez, G. S. Duesberg, N. McEvoy, T. J. Pennycook, C. Downing, A. Crossley, V. Nicolosi and J. N. Coleman, *Nat. Mater.*, 2014, **13**, 624–630.
22 H. C. Schniepp, J. L. Li, M. J. McAllister, H. Sai, M. Herrera-Alonso, D. H. Adamson, R. K. Prud'homme, R. Car, D. A. Saville and I. A. Aksay, *J. Phys. Chem. B*, 2006, **110**, 8535–8539.
23 M. J. McAllister, J. L. Li, D. H. Adamson, H. C. Schniepp, A. A. Abdala, J. Liu, M. Herrera-Alonso, D. L. Milius, R. Car, R. K. Prud'homme and I. A. Aksay, *Chem. Mater.*, 2007, **19**, 4396–4404.
24 L. Staudenmaier, *Ber. Dtsch. Chem. Ges.*, 1898, **31**, 1481–1487.
25 U. Hofmann and E. Konig, *Z. Anorg. Allg. Chem.*, 1937, **234**, 311.
26 W. S. Hummers and R. E. Offeman, *J. Am. Chem. Soc.*, 1958, **80**, 1339–1339.
27 D. C. Marcano, D. V. Kosynkin, J. M. Berlin, A. Sinitskii, Z. Z. Sun, A. Slesarev, L. B. Alemany, W. Lu and J. M. Tour, *ACS Nano*, 2010, **4**, 4806–4814.
28 S. J. You, S. M. Luzan, T. Szabo and A. V. Talyzin, *Carbon*, 2013, **52**, 171–180.
29 F. Kim, J. Y. Luo, R. Cruz-Silva, L. J. Cote, K. Sohn and J. X. Huang, *Adv. Funct. Mater.*, 2010, **20**, 2867–2873.
30 I. K. Moon, J. Lee, R. S. Ruoff and H. Lee, *Nat. Commun.*, 2010, **1**, 73.
31 Z. Sofer, P. Simek and M. Pumera, *Phys. Chem. Chem. Phys.*, 2013, **15**, 9257–9264.
32 C. Z. Zhu, S. J. Guo, Y. X. Fang and S. J. Dong, *ACS Nano*, 2010, **4**, 2429–2437.
33 H.-L. Guo, X.-F. Wang, Q.-Y. Qian, F.-B. Wang and X.-H. Xia, *ACS Nano*, 2009, **3**, 2653–2659.
34 J. Chen, B. Yao, C. Li and G. Shi, *Carbon*, 2013, **64**, 225–229.
35 N. Liu, F. Luo, H. Wu, Y. Liu, C. Zhang and J. Chen, *Adv. Funct. Mater.*, 2008, **18**, 1518–1525.
36 A. K. Geim, *Science*, 2009, **324**, 1530–1534.
37 Y. C. Si and E. T. Samulski, *Nano Lett.*, 2008, **8**, 1679–1682.
38 S. Park, J. H. An, I. W. Jung, R. D. Piner, S. J. An, X. S. Li, A. Velamakanni and R. S. Ruoff, *Nano Lett.*, 2009, **9**, 1593–1597.
39 S. Park, J. H. An, R. D. Piner, I. Jung, D. X. Yang, A. Velamakanni, S. T. Nguyen and R. S. Ruoff, *Chem. Mater.*, 2008, **20**, 6592–6594.
40 M. Zhang, R. R. Parajuli, D. Mastrogiovanni, B. Dai, P. Lo, W. Cheung, R. Brukh, P. L. Chiu, T. Zhou, Z. F. Liu, E. Garfunkel and H. X. He, *Small*, 2010, **6**, 1100–1107.
41 M. Lotya, Y. Hernandez, P. J. King, R. J. Smith, V. Nicolosi, L. S. Karlsson, F. M. Blighe, S. De, Z. Wang, I. T. McGovern, G. S. Duesberg and J. N. Coleman, *J. Am. Chem. Soc.*, 2009, **131**, 3611–3620.
42 K. H. Park, B. H. Kim, S. H. Song, J. Kwon, B. S. Kong, K. Kang and S. Jeon, *Nano Lett.*, 2012, **12**, 2871–2876.
43 A. C. Jachak, M. Creighton, Y. Qiu, A. B. Kane and R. H. Hurt, *MRS Bull.*, 2012, **37**, 1307–1313.
44 V. C. Sanchez, A. Jachak, R. H. Hurt and A. B. Kane, *Chem. Res. Toxicol.*, 2012, **25**, 15–34.

45 V. Sridhar, J.-H. Jeon and I.-K. Oh, *Carbon*, 2010, **48**, 2953–2957.
46 P. L. Chiu, D. Mastrogiovanni, D. Wei, C. Louis, M. Jeong, G. Yu, P. Saad, C. R. Flach, R. Mendelsohn, E. Garfunkel and H. X. He, *J. Am. Chem. Soc.*, 2012, **134**, 5850–5856.
47 M. A. Patel, H. Yang, P. L. Chiu, D. Mastrogiovanni, C. R. Flach, K. Savaram, L. Gomez, A. Hemnarine, R. Mendelsohn, E. Garfunkel, H. Jiang and H. X. He, *ACS Nano*, 2013, **7**, 8147–8157.
48 K. J. Ziegler, Z. N. Gu, H. Q. Peng, E. L. Flor, R. H. Hauge and R. E. Smalley, *J. Am. Chem. Soc.*, 2005, **127**, 1541.
49 J. Liu, A. G. Rinzler, H. J. Dai, J. H. Hafner, R. K. Bradley, P. J. Boul, A. Lu, T. Iverson, K. Shelimov, C. B. Huffman, F. Rodriguez-Macias, Y. S. Shon, T. R. Lee, D. T. Colbert and R. E. Smalley, *Science*, 1998, **280**, 1253–1256.
50 A. M. Dimiev, S. M. Bachilo, R. Saito and J. M. Tour, *ACS Nano*, 2012, **6**, 7842–7849.
51 V. T. Tung, M. J. Allen, Y. Yang and R. B. Kaner, *Nat. Nanotechnol.*, 2009, **4**, 25–29.
52 H. A. Becerril, J. Mao, Z. F. Liu, R. M. Stoltenberg, Z. Bao and Y. S. Chen, *ACS Nano*, 2008, **2**, 463–470.
53 Y. Hernandez, M. Lotya, D. Rickard, S. D. Bergin and J. N. Coleman, *Langmuir*, 2010, **26**, 3208–3213.
54 A. Bagri, C. Mattevi, M. Acik, Y. J. Chabal, M. Chhowalla and V. B. Shenoy, *Nat. Chem.*, 2010, **2**, 581–587.
55 G. Eda, G. Fanchini and M. Chhowalla, *Nat. Nanotechnol.*, 2008, **3**, 270–274.
56 D. Briggs and G. Beamson, *High Resolution XPS of Organic Polymers: The Scienta ESCA300 Database Appendix I*, John Wiley & Sons Ltd, 1992.
57 G. E. Pike and C. H. Seager, *Phys. Rev. B: Solid State*, 1974, **10**, 1421–1434.
58 H. Chen, M. B. Muller, K. J. Gilmore, G. G. Wallace and D. Li, *Adv. Mater.*, 2008, **20**, 3557–3561.
59 A. Bagri, R. Grantab, N. V. Medhekar and V. B. Shenoy, *J. Phys. Chem. C*, 2010, **114**, 12053–12061.
60 A. M. Dimiev and J. M. Tour, *ACS Nano*, 2014, **8**, 3060–3068.
61 T. H. Han, Y. K. Huang, A. T. L. Tan, V. P. Dravid and J. X. Huang, *J. Am. Chem. Soc.*, 2011, **133**, 15264–15267.
62 *Microwave-Enhanced Chemistry: Fundamentals, Sample Preparation, and Applications*, ed. H. M. (Skip) Kingston and S. J. Haswell, American Chemical Society, Washington, DC, 1997.
63 J. Zhang, H. L. Zou, Q. Qing, Y. L. Yang, Q. W. Li, Z. F. Liu, X. Y. Guo and Z. L. Du, *J. Phys. Chem. B*, 2003, **107**, 3712–3718.
64 Wikipedia, 2014.
65 J. F. de Queiroz, J. W. D. Carneiro, A. A. Sabino, R. Sparrapan, M. N. Eberlin and P. M. Esteves, *J. Org. Chem.*, 2006, **71**, 6192–6203.
66 P. M. Esteves, J. W. D. Carneiro, S. P. Cardoso, A. G. H. Barbosa, K. K. Laali, G. Rasul, G. K. S. Prakash and G. A. Olah, *J. Am. Chem. Soc.*, 2003, **125**, 4836–4849.